Electrostatic modeling of intracloud stepped leader electric fields and mechanisms of terrestrial gamma ray flashes

Victor P. Pasko[1]

[1]CSSL Laboratory, Department of Electrical Engineering, Pennsylvania State University, University Park, Pennsylvania, USA

Abstract Understanding of electric field configurations created by long intracloud (IC) stepped leaders is of significant interest for understanding how these events produce bursts of high-energy photons in the Earth's atmosphere, commonly referred to as terrestrial gamma ray flashes (TGFs). In the present work modeling results using the electrostatic moment method solutions are used for quantitative interpretation of electric fields observed at close ~200 m and long ~30 km ranges from IC stepped leaders. The modeling results are consistent with the existence and continuous advancement of VHF-dark positive leaders at the positive end of the bidirectional leader system. It is demonstrated that the electric dipole moment of the entire leader system is a quadratic function of the leader length, and the dipole moment changes due to the leader steps increase proportionally to the overall leader length (i.e., even when step length remains constant), in good agreement with observations. The results indicate that the dipole moment changes on the order of tens of C km and current moment changes on the order of tens of kA km, that have been associated with TGFs, are essential attributes of long IC stepped leaders and directly follow from their intrinsic large-scale charge dynamics.

1. Introduction

Winn et al. [2011] have reported time-resolved observations of electric field components parallel and perpendicular to the intracloud (IC) stepped leader that passed within 200 m of a balloon-borne electric field change instrument at 9.1 km altitude and covered total length of ~11.6 km, with an average velocity of ~10^5 m/s. The stepping distances ranged between 50 m and 600 m and during each step the electric field component perpendicular to the channel exhibited a fast (during several tens of microseconds) decrease on the order of 2 kV/m followed by a slow recovery. The goal of the present paper is to report quantitative modeling results allowing interpretation of these observations using the electrostatic moment method solutions for charges induced on a long (overall charge neutral) conducting leader channel placed in an external electric field. The results are also applied to quantitative interpretation of quasi-static electric field changes observed at horizontal distances ~30 km from long intracloud lightning leaders with characteristics believed to be responsible for production of terrestrial gamma ray flashes (TGFs) [*Marshall et al.*, 2013].

2. Charge Distributions on Long Leaders

A leader as an overall electrostatic system can be approximated as a long perfectly conducting wire of length *L* as depicted in Figure 1. Assuming downward applied electric field with magnitude E_0 as shown in Figure 1, it is expected that the wire will be polarized with negative charge $-Q$ induced on the upper end and equal amount of positive charge $+Q$ on the lower end. The actual charge distribution can be represented using a linear charge density that is highly inhomogeneous function along the leader length, with strong peaks at the ends [e.g., *Mazur and Ruhnke*, 1998] (see also distributions in Figure 3a of the present paper). An observer positioned at some location in the immediate vicinity of the wire channel would see electric field that is mostly normal to the wire and is defined by the local linear charge density at that location. For a constant applied electric field the linear charge density is always exactly symmetric with respect to the center of the wire (i.e., the neutral point) where the charge density is equal to zero. If one of the ends of the wire lengthens (i.e., during stepping of the negative leader), a stationary observer positioned next to that end, near the channel, would generally see a reduction in electric field component normal to the wire simply because the charge enhancement at the end of the wire shifts away from the observer, and the observer now appears to be positioned closer to the neutral point of the wire. Similarly, a slow subsequent growth of the opposite end of the wire would lead to the electric field recovery as seen by the observer at
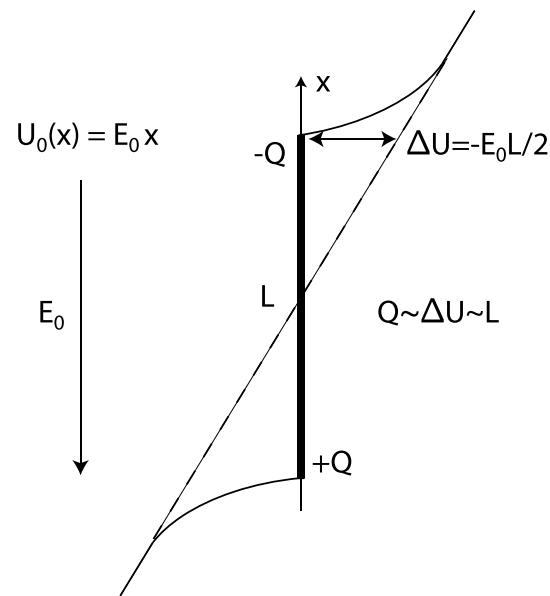
Figure 1. Schematic representation of a leader as a long conductor [*Bazelyan and Raizer*, 2000, p. 54].

the same location. It is suggested that these dynamics are responsible for principal aspects of the electric field waveforms reported in *Winn et al.* [2011, Figures 5–7], as will be quantified below in this paper.

The tips of the same wire (see Figure 1) form potential differences with respect to ambient potential, of magnitude $\Delta U = E_0 L / 2$ [*Bazelyan and Raizer*, 2000, p. 54], which are proportional to the leader length L. Since $\Delta U \sim Q$, where Q is magnitude of charge induced on the wire as discussed at the beginning of this section, the overall dipole moment of the entire leader system is a quadratic function of the leader length $P = QL \sim L^2$. The electric field seen by a remote observer is proportional to the dipole moment P and also scales $\sim L^2$ with the leader length (in particular, would increase as a square of time for a leader propagating with constant speed). A short leader (for example a space leader forming during steps of the negative leader), with length $L_s \ll L$ that is electrically separated from the main leader channel, would not produce a significant electric field at large distances, while the new dipole moment after the electrical connection and extension of the main leader channel by increment L_s is $P_{new} \sim (L + L_s)^2 \sim L^2 + 2LL_s$, assuming $L_s \ll L$. The new dipole moment can therefore be expressed as $P_{new} = P + \Delta P$, where $\Delta P \sim L$. Therefore, even when step distance L_s remains constant, the dipole moment and electric field changes seen by a remote observer increase proportionally to overall leader length L. The increase in the dipole moment and electric field changes in the course of leader propagation is illustrated by numerous examples in *Marshall et al.* [2013] and will be further quantified in the context of modeling presented in this paper.

3. Model Formulation

Typical experimentally measured ambient field values in which intracloud leaders propagate are on the order of 10–50 kV/m [e.g., *Winn et al.*, 2011; *Marshall et al.*, 2001, 2013]. In the present work an intracloud stepped leader is modeled as a vertical perfectly conducting cylinder with radius 1 cm [*Rakov and Uman*, 2003, p. 134] propagating in downward directed external electric field with magnitude $E_0 = 50$ kV/m (Figure 2a). The model leader is assumed to initiate at altitude 6.5 km and develop as a bidirectional system [*Mazur and Ruhnke*, 1998] with downward positive leader head advancing continuously with speed v_L and upward negative leader head advancing by periodic steps of length L_s that form with speed v_s. The negative leader is not allowed to propagate between steps and periodicity of steps is chosen so that at the time instants right after formation of negative leader steps the overall lengths of positive and negative leader sections with respect to the initiation point are equal (i.e., the time average speeds of spatial growth of both positive and negative leader heads are assumed to be the same and equal to v_L). In the present work the results are presented for two separate sets of parameters: $v_L = 10^5$ m/s, L_s=200 m, $v_s = 10v_L = 10^6$ m/s; and $v_L = 5 \times 10^5$ m/s, L_s=1000 m, $v_s = 10v_L = 5 \times 10^6$ m/s. The first set is consistent with conditions reported in *Winn et al.* [2011] when a ~10 km long leader is formed on a time scale of ~100 ms (average speed
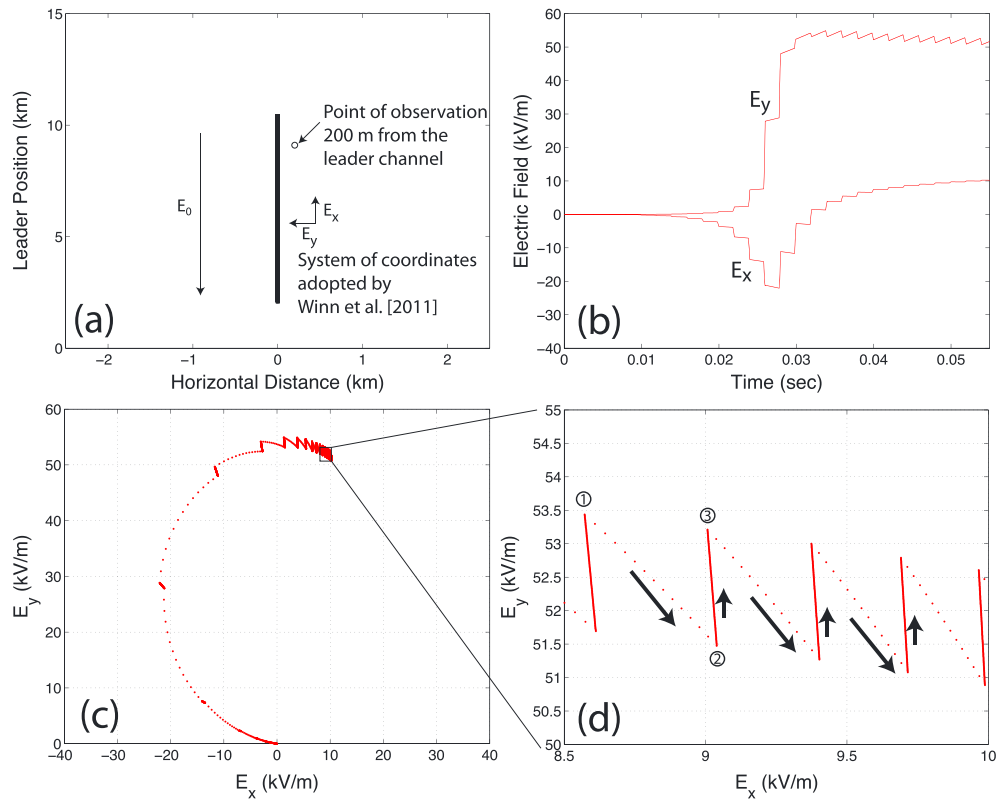
Figure 2. (a) Model leader geometry and coordinate system used in the present study. (b) The x and y components of the electric field calculated at 9.1 km altitude and 200 m horizontal distance from the model leader developing with average velocity $v_L = 10^5$ m/s and step length $L_s = 200$ m. (c) The E_x-E_y diagram corresponding to Figure 2b showing time dynamics of the tip of the electric field vector with step 14.2 μs. (d) Zoom in view corresponding to Figure 2c.

$\sim 10^5$ m/s). The second set, corresponding to a factor of 5 greater leader speed, is relevant to conditions of relatively fast propagation of leaders reported in *Marshall et al.* [2013] and *Lu et al.* [2010, 2011], where leader extended overall vertical distances $\sim$5 km in $\leq$10 ms. For example, the flash A documented in *Marshall et al.* [2013, Figure 3] extended 4.2 km, from 7.3 km to 11.5 km, in $\sim$7 ms (overall estimated speed $\sim 6 \times 10^5$ m/s) and contained three distinct fast steps with estimated lengths 1.2 km, 1.7 km, and 1 km that developed with speeds 6×10^6 m/s, 8.5×10^6 m/s, and 1.7×10^6 m/s, respectively.

The solution for charges induced on the leader depicted in Figure 2a is found by using the method of moments [*Balanis*, 1989, p. 670]. The approach closely follows those recently developed for calculations of electric fields and potential differences developing near tips of long lightning leaders that lead to ter-restrial gamma ray flashes (TGFs) [e.g., *Celestin et al.*, 2012, and references cited therein]. An isolated long conducting wire centered at $x = 0$ and placed in external electric field $\vec{E} = -\vec{i}_x E_0$ (corresponding potential $U_0(x) = E_0 x$) is assumed to be equipotential and overall charge neutral. The potential distribution describ-ing charges induced on the wire can therefore be approximated as $U_{ind}(x) = -U_0(x)$ and directly used as a boundary condition on the surface of the wire to obtain corresponding linear charge distribution induced on the wire [*Balanis*, 1989, p. 670]. Figure 3a illustrates related distributions that will be discussed below. The charge distributions can then be used to tabulate electric field components parallel and perpendicu-lar to the wire at any location in space. For direct comparison with experimental measurements reported in *Winn et al.* [2011] in the present work the field solutions are presented using coordinate system depicted in Figure 2a with x axis parallel to the leader and y axis pointing toward the leader. Also the point of obser-vation is placed at 9.1 km altitude and 200 m from the leader axis (see Figure 2a). We note that although the leader experimentally observed by *Winn et al.* [2011] had a significant tilt with respect to vertical (i.e., exhibited significant horizontal propagation component), the results we present are not sensitive to leader orientation since we express them in the frame of reference linked to the leader channel that is identical to the one used by *Winn et al.* [2011]. An advantage of keeping the model leader vertical is that using the same
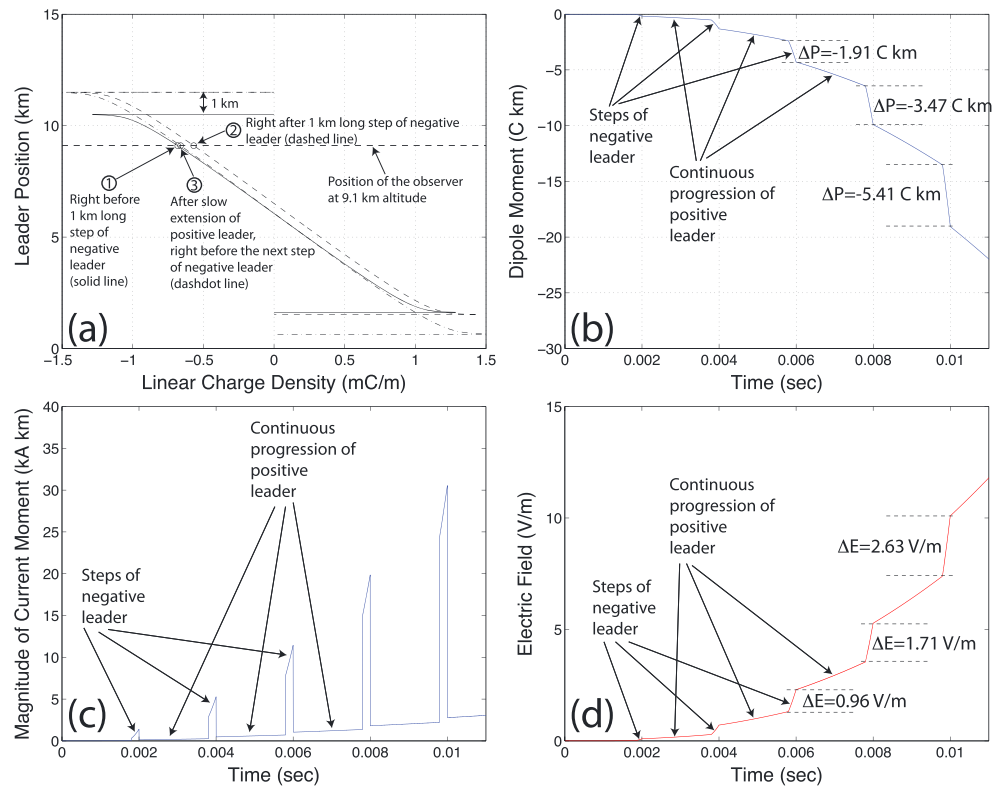
Figure 3. (a) Linear charge density distribution on model leader at representative time instances marked in the figure. The horizontal dashed line marks position of the observer at 9.1 km altitude. (b) Dipole moment as a function of time for a model leader developing with average velocity $v_L = 5 \times 10^5$ m/s and step length L_s=1000 m. (c) Magnitude of the current moment corresponding to results shown in Figure 3b. The vertical component of electric field on the ground at 30 km horizontal distance corresponding to results shown in Figure 3b.

model, one can also directly compare to electric fields observed at large horizontal distances on the ground as relevant to observations reported in *Marshall et al.* [2013] and *Lu et al.* [2010, 2011]. We present related results assuming horizontal distance 30 km, similar to that in observations reported by *Marshall et al.* [2013]. At these distances contribution of image charges associated with the conducting ground is essential, and all presented model results for electric fields account for the ground images.

4. Results

Figures 2b–2d present model results for the first set of parameters (for $v_L = 10^5$ m/s) in the format identical to that reported in *Winn et al.* [2011, Figures 5–7]. As a negatively charged stepped leader channel approaches point of observation from below (see Figure 2a) the observer sees a negative E_x field component and increasing positive E_y component. The E_y component peaks at around 55 kV/m and E_x at ~ −22 kV/m. After the leader head passes the point of closest approach, the E_x field polarity reverses. Although actual leader channel likely significantly deviated from the linear model representation, the model dynamics agrees with observations well in terms of field magnitudes, polarities, and time dynamics. *Winn et al.* [2011] suggested a charge distribution in the top panel of their Figure 6 based on a model by *Mazur and Ruhnke* [1998] with a linear charge density peaking at ~ −1 mC/m in the leader head. The charge distribution obtained in the present modeling (see Figure 3a) is fully consistent with this previous modeling and produces similar results for electric field components and dynamics.

Figure 2d shows a zoom in view of the electric field dynamics after the negative leader head passed the point of observation (similar to *Winn et al.* [2011, Figure 7]). The characteristic dynamics involve fast reduction of E_y during steps of negative leader (marked by a long downward arrow aligned in Figure 2d, 1-2 path), followed by slow recovery (path 2-3 with short upward arrow). Figure 3a, based on a second set of parameters (i.e., for additional clarity a case with 1 km leader steps is used for discussion here), provides a conceptual explanation of the observed field dynamics. Right after the 1 km long leader step (from point in

time marked 1 to point 2) the overall charge in the negative leader head shifts upward resulting in observer (position marked by horizontal dashed line at 9.1 km) being positioned next to the region of the lower charge density on the channel and therefore seeing a lower E_y electric field value. Note also upward shift of the neutral point on the channel right after the step of the negative leader. The field seen by the observer then slowly recovers (from point 2 to point in time marked 3) as positive end of the positive leader continues its downward propagation.

Figure 3b documents dynamics of the dipole moment of the overall leader system for the second set of model parameters (i.e., $v_L = 5 \times 10^5$ m/s, $L_s = 1000$ m, $v_s = 10v_L = 5 \times 10^6$ m/s). As predicted on the basis of analytic theory in section 2 the dipole moment changes during steps of negative leader progressively increase, even though the steps remain constant. The direct time differentiation of the dipole moment in Figure 3b gives the time dynamics of the magnitude of the current moment shown in Figure 3c with peak values on the order of several tens of kA km. Figure 3d documents time dynamics of the vertical electric field as would be observed on the ground at 30 km horizontal distance corresponding to dipole moment dynamics shown in Figure 3b. We note a progressive increase in electric field changes during steps of the negative leader, very similar to cases reported recently by *Marshall et al.* [2013, Figure 3 and Table 3].

5. Discussion

We note that the modeling approach adopted in this paper relies on a relatively small number of input parameters that include magnitude of the ambient electric field, overall length of the leader, and the leader speed; all of which can be reasonably approximated using available experimental data as discussed in the previous sections. The reported results depend on the assumed radius of the leader channel (1 cm) that would affect the capacitance of the channel. However, we note that the dependence on radius is generally weak since it follows a logarithmic law (see equation (7), for instance, in, e.g., *Mazur and Ruhnke* [1998, and references therein]). For example, adopting a hundred times greater leader radius, i.e., 1 m as proposed in *Mazur and Ruhnke* [1998], effectively leads to an approximate increase in channel capacitance by a factor of 1.65, and all physical quantities shown in Figures 2b–2d and 3 (all panels) can be directly rescaled by multiplying by this factor. Alternatively, we have verified that all numerical values shown in Figures 2b–2d and 3 (all panels) will remain approximately the same if one assumes a factor of 1.65 lower ambient applied field $E_0 = 50 / 1.65$ kV/m $\simeq 30$ kV/m. This would reduce voltage differences induced on the channel that in combination with increased capacitance would preserve the same induced charge on the channel (these results are not included here for the sake of brevity). More significantly, the capacitance would also be affected by branching of the channel. The replacement of a long vertical section of the positive leader end with a shorter but more branched leader system may increase capacitance of the leader system and overall charge and dipole moments in comparison with those reported in the present work. Also, in the immediate vicinity of the leader channel it is expected that streamer corona would lead to effective spatial spreading of the charge distributions in comparison with simple linear charge distributions adopted in the reported modeling. Nevertheless, the presented comparison of model results with quasi-static fields observed at relatively close, ~100 m, [*Winn et al.*, 2011] and large, about tens of kilometers, [*Marshall et al.*, 2013] ranges indicates that the present model correctly captures principal large-scale charge configurations of IC lightning leaders, at least in some of the cases.

As was already noted above the time intervals marked as continuous progression of positive leader in Figures 3b–3d agree very well with dynamics documented in observations reported by *Marshall et al.* [2013]. Also, as demonstrated by the present modeling, these episodes link very well with slow field recovery stages reported by *Winn et al.* [2011] (see discussion related to Figures 2d and 3a). It is remarkable in this context that neither *Winn et al.* [2011] nor *Marshall et al.* [2013] reported any experimental detection of these positive leaders during development of the negative leaders. In both cases, some VHF activity/*K* waves at lower altitudes possibly indicating reillumination of previously propagated positive leaders have been observed at times ≥100 ms after the detection of negative leaders [*Winn et al.*, 2011; *Marshall et al.*, 2013]. *Marshall et al.* [2013] states, in particular, that their data show no evidence of positive leaders developing simultaneously with the initial negative leaders. They also point that this does not mean that there were no positive leaders present. *Winn et al.* [2011] emphasize in their introduction that positive leaders radiate weakly and might be missed by the Lightning Mapping Array. The modeling study reported in this paper may be considered as an additional evidence indicating that VHF-dark positive leaders (i.e., those not producing detectable VHF radiation) indeed were present simultaneously with the negative leaders (see additional discussion in *Rison*

et al. [1999]). We emphasize that the main assumption of the modeling as applied to results reported in *Marshall et al.* [2013] is that lightning has already been initiated (i.e., a hot propagating leader channel has been created [*Dwyer and Uman*, 2013, section 3]).

Winn et al. [2011] point out that the time intervals corresponding to formation of leader steps (i.e., those shown by fast reduction of E_y electric field component in *Winn et al.* [2011, Figure 7] or analogous model representations shown by downward arrows and with the same time step 14.2 μs in Figure 2d of the present paper) is very long, exceeding ∼100 μs, and do not resemble fast processes expected to proceed on time scales ∼5 μs typically observed in stepped leaders near the ground. In this context we note that the actual electrical connection between space leader and the main leader in the negative stepped leader advancement process may be nearly instantaneous. However, formation of new electrostatic charge configuration on a long leader that is measured by *Winn et al.* [2011] at one fixed location near the leader channel requires propagation of transient waves of potential and charge along the leader. Having assumed a typical return stroke speed on the order of one tenth of speed of light, it would take at least ∼100 μs to cover distance of 3 km. Although the present electrostatic modeling does not allow to reproduce related dynamics, it is likely that the simple geometry involving very long leaders is responsible for the extended time periods, as seen by local observer at some location near the channel, to complete new charge configuration hundreds of μs after actual leader step was formed. The data recently published by *Marshall et al.* [2013] indicate that in addition to progressive growth of observed dipole moment changes during leader steps as already discussed above, it also takes a progressively longer time to establish each dipole moment change. Given the above discussion this also may be considered as a direct reflection of overall growth of the leader length.

In context of understanding of mechanisms of terrestrial gamma ray flashes (TGFs), results of *Winn et al.* [2011] are of special interest as they provide better understanding of step phenomenology and temporal evolution of large-scale charge distributions on long IC lightning leaders. The present results indicate that the dipole moment changes on the order of tens of C km and current moment changes on the order of tens of kA km that have been associated with TGFs [*Cummer et al.*, 2005; *Lu et al.*, 2010, 2011] are essential attributes of long stepped leaders and directly follow from their intrinsic large-scale charge dynamics. We emphasize that during each step the charge redistribution on the entire, many kilometers long, leader channel contributes to creation of large dipole and current moment changes (see Figure 3a, for example). In this context recently reported correlations of strong VLF emissions and TGFs [*Connaughton et al.*, 2010, 2013] may be an indication of the overall strength of IC leader to produce both effects and not necessarily an indication that currents associated with runaway electrons producing TGFs [*Dwyer and Cummer*, 2013] are directly responsible for the VLF emissions. Actual TGF source may be confined to a relatively compact region around negative leader tip [*Celestin and Pasko*, 2011; *Xu et al.*, 2012]. *Ostgaard et al.* [2013] recently reported simultaneous observations of optical lightning signal and TGF event indicating that TGF was produced during the initial stage of an IC lightning before the leader reached the cloud top and extended horizontally.

It is interesting to note in this context that the model leader length at the time $t = 0.02$ s shown in Figure 2b is exactly $L = 4$ km, giving potential difference in the leader head $\Delta U = E_0 L/2 = 100$ MV. This is fully sufficient to support energetics of observed TGFs [e.g., *Mallios et al.*, 2013, and references cited therein]. The model ΔU continues to increase proportionally to time (i.e., doubles by $t = 0.04$ s). Assuming the threshold field for the relativistic runaway electron avalanche to be $E_t = 280$ kV/m at ground level [*Dwyer*, 2008], the same field scaled with atmospheric density is estimated to be 98 kV/m at 9.1 km considered in the present work. We note that the total model electric field at 200 m distance from the leader head at 9.1 km altitude (i.e., formed by components shown in Figure 2a plus ambient −50 kV/m contributing to the x component) never exceeds 80 kV/m and therefore remains $< E_t$ at that location. The total negative charge around the leader head shown on Figure 3a is on the order of ∼ −2 C (i.e., ∼1 mC/m × ∼2 km). *Marshall et al.* [2013] recently used similar experimentally inferred point charge of −2.1 C to estimate electric field 72 kV/m at distance 500 m above the leader tip that jointly with the 50 kV/m ambient field (i.e., 122 kV/m) significantly exceeded the $E_t = 86$ kV/m, at 9.5 km altitude considered. We emphasize in context of the modeling presented in the present work that point charge geometry assumed by *Marshall et al.* [2013] may lead to a significant overestimation of electric field magnitudes, in comparison with more realistic cases when the same charge is distributed on a several kilometer long channel.

References

Balanis, C. A. (1989), *Advanced Engineering Electromagnetics*, John Wiley, New York.

Bazelyan, E. M., and Y. P. Raizer (2000), *Lightning Physics and Lightning Protection*, IoP Publishing Ltd, Bristol, U.K., and Philadelphia, Pa.

Celestin, S., and V. P. Pasko (2011), Energy and fluxes of thermal runaway electrons produced by exponential growth of streamers during the stepping of lightning leaders and in transient luminous events, *J. Geophys. Res.*, *116*, A03315, doi:10.1029/2010JA016260.

Celestin, S., W. Xu, and V. P. Pasko (2012), Terrestrial gamma ray flashes with energies up to 100 MeV produced by nonequilibrium acceleration of electrons in lightning, *J. Geophys. Res.*, *117*, A05315, doi:10.1029/2012JA017535.

Connaughton, V., et al. (2010), Associations between Fermi Gamma-ray Burst Monitor terrestrial gamma ray flashes and sferics from the World Wide Lightning Location Network, *J. Geophys. Res.*, *115*, A12307, doi:10.1029/2010JA015681.

Connaughton, V., et al. (2013), Radio signals from electron beams in terrestrial gamma ray flashes, *J. Geophys. Res. Space Physics*, *118*, 2313–2320, doi:10.1029/2012JA018288.

Cummer, S. A., Y. Zhai, W. Hu, D. M. Smith, L. I. Lopez, and M. A. Stanley (2005), Measurements and implications of the relationship between lightning and terrestrial gamma ray flashes, *Geophys. Res. Lett.*, *32*, L08811, doi:10.1029/2005GL022778.

Dwyer, J. R. (2008), Source mechanisms of terrestrial gamma-ray flashes, *J. Geophys. Res.*, *113*, D10103, doi:10.1029/2007JD009248.

Dwyer, J. R., and S. A. Cummer (2013), Radio emissions from terrestrial gamma ray flashes, *J. Geophys. Res. Space Physics*, *118*, 3769–3790, doi:10.1002/jgrd.50188.

Dwyer, J. R., and M. A. Uman (2013), The physics of lightning, *Phys. Rep.*, doi:10.1016/j.physrep.2013.09.004.

Lu, G., R. J. Blakeslee, J. Li, D. M. Smith, X. M. Shao, E. W. McCaul, D. E. Buechler, H. J. Christian, J. M. Hall, and S. A. Cummer (2010), Lightning mapping observation of a terrestrial gamma-ray flash, *Geophys. Res. Lett.*, *37*, L11806, doi:10.1029/2010GL043494.

Lu, G., S. A. Cummer, J. Li, F. Han, D. M. Smith, and B. W. Grefenstette (2011), Characteristics of broadband lightning emissions associated with terrestrial gamma ray flashes, *J. Geophys. Res.*, *116*, A03316, doi:10.1029/2010JA016141.

Mallios, S. A., S. Celestin, and V. P. Pasko (2013), Production of very high potential differences by intracloud lightning discharges in connection with terrestrial gamma ray flashes, *J. Geophys. Res. Space Physics*, *118*, 912–918, doi:10.1002/jgra.50109.

Marshall, T., M. Stolzenburg, S. Karunarathne, S. Cummer, G. Lu, H.-D. Betz, M. Briggs, V. Connaughton, and S. Xiong (2013), Initial breakdown pulses in intracloud lightning flashes and their relation to terrestrial gamma ray flashes, *J. Geophys. Res. Atmos.*, *118*, 10,907–10,925, doi:10.1002/jgrd.50866.

Marshall, T. C., M. Stolzenburg, W. D. Rust, E. R. Williams, and R. Boldi (2001), Positive charge in the stratiform cloud of a mesoscale convective system, *J. Geophys. Res.*, *106*(D1), 1157–1164, doi:10.1029/2000JD900625.

Mazur, V., and L. H. Ruhnke (1998), Model of electric charges in thunderstorms and associated lightning, *J. Geophys. Res.*, *103*(D18), 23,299–23,308.

Ostgaard, N., T. Gjesteland, B. E. Carlson, A. B. Collier, S. A. Cummer, G. Lu, and H. J. Christian (2013), Simultaneous observations of optical lightning and terrestrial gamma ray flash from space, *Geophys. Res. Lett.*, *40*, 2423–2426, doi:10.1029/grl.50466.

Rakov, V. A., and M. A. Uman (2003), *Lightning: Physics and Effects*, Cambridge Univ. Press, Cambridge, U.K., and New York.

Rison, W., R. J. Thomas, P. R. Krehbiel, T. Hamlin, and J. Harlin (1999), A GPS-based three-dimensional lightning mapping system: Initial observations in central New Mexico, *Geophys. Res. Lett.*, *26*(23), 3573–3576, doi:10.1029/1999GL010856.

Winn, W. P., G. D. Aulich, S. J. Hunyady, K. B. Eack, H. E. Edens, P. R. Krehbiel, W. Rison, and R. G. Sonnenfeld (2011), Lightning leader stepping, K changes, and other observations near an intracloud flash, *J. Geophys. Res.*, *116*, D23115, doi:10.1029/2011JD015998.

Xu, W., S. Celestin, and V. P. Pasko (2012), Source altitudes of terrestrial gamma-ray flashes produced by lightning leaders, *Geophys. Res. Lett.*, *39*, L08801, doi:10.1029/2012GL051351.